Contrib Mineral Petrol (1988) 99:249–256

Contributions to Mineralogy and Petrology

The Gibbs method and Duhem's theorem: The quantitative relationships among *P*, *T*, chemical potential, phase composition and reaction progress in igneous and metamorphic systems

Frank S. Spear
Department of Geology, Rensselaer Polytechnic Institute, Troy, New York 12180, USA

Abstract. The Gibbs method permits simultaneous evaluation of the relationships among all intensive thermodynamic variables of a heterogeneous system in equilibrium. Addition of mass balance constraints permits simultaneous evaluation of both intensive and extensive variables so that changes in phase chemistry and modes may be monitored. Assumption of closed system behavior results in a system of equations with two degrees of freedom, regardless of the thermodynamic variance, as specified by Duhem's theorem. Open system behavior increases the number of degrees of freedom by the number of components to which the system is open. The methodology presented is therefore a formal statement of the constraints among the differential of all of the intensive and extensive variables of a heterogeneous system.

Examples of the application of this formalism include contouring pressure-temperature space for mineral composition, modal changes and reaction progress; contouring reaction space with pressure, temperature and mineral composition; and calculation of compositional and modal changes of phases for prescribed changes in pressure and temperature, as, for example, in the calculation of synthetic garnet zoning profiles or liquid lines of descent in crystallizing magmas.

Introduction

The texture and chemistry of a rock exposed at the surface is in part a function of the changes in external conditions (e.g. *P*, *T*, $a(H_2O)$, etc.) that the rock has experienced. A goal of the petrologist is to determine the particular changes in external conditions that have resulted in the observed texture, mineralogy, and mineral chemistry of the rock.

The purpose of this paper is to present a methodology that may be of some assistance to the petrologist in the interpretation of reaction textures and mineral chemistries. The method involves a thermodynamic formalism known as the Gibbs method (Spear et al. 1982) that permits simultaneous calculation of changes in intensive (e.g. *P*, *T* and mineral composition) and extensive (e.g. modes) thermodynamic parameters of a heterogeneous system in equilibrium. The technique described here represents an extension of earlier treatments of the Gibbs method (e.g. Spear et al. 1982; Spear and Selverstone 1983) in that the earlier treatments incorporated only the intensive variables *P*, *T*, μ (chemical potential) and *X* (composition). The present study permits consideration of extensive variables *M* (modes or moles of phases present) through the addition of mass balance constraints.

This formalism may be applied to the contouring of $P-T$ space for changes in mineral composition or mineral abundance. Alternatively, because reaction progress can be defined in terms of the production or destruction of a phase, the formalism may be applied to the contouring of reaction space (Thompson 1982) for *P*, *T* and mineral composition. These contour diagrams may aid in the interpretation of observations such as textural criteria as to whether a phase is being produced or consumed or the compositional history of minerals in the rock as inferred from chemical zoning or the compositions of mineral inclusions. Examples from simple igneous and metamorphic systems will be given.

Theory

The theoretical framework involves application of the concepts embodied in Duhem's theorem to the formalism of the Gibbs method (Spear et al. 1982). The Gibbs method relates all intensive parameters of a heterogeneous system in equilibrium through a system of linear differential equations. These equations have been derived elsewhere (e.g. Spear et al. 1982), but briefly they include (1) a Gibbs-Duhem equation for each phase in the assemblage:

$$0 = S\,dT - V\,dP + \Sigma X_j\,d\mu_j \tag{1}$$

(2) a set of linearly independent stoichiometric relations written among differentials of the chemical potentials of the phase components:

$$0 = \Sigma \nu_i\,\mu_i \tag{2}$$

and (3) equations that relate changes in the chemical potential of independently variable phase components to changes in composition through the curvatures and cross curvatures of the Gibbs free energy function:

$$0 = -(d\mu_i - d\mu_d) - (S_i - S_d)\,dT + (V_i - V_d)\,dP + \Sigma(\partial^2 G/\partial X_i\,\partial X_j)_{P,T}\,dX_i \tag{3}$$

where the subscript *d* refers to the dependent phase component, S_i and V_i are partial molar entropies and volumes, and the summation is over all independent phase components. The equations (1), (2) and (3) represent formal relations among the intensive variables dT, dP, $d\mu$ and dX

in a heterogeneous system at equilibrium. Because the Gibbs method relates only intensive variables of a heterogeneous system, this methodology is best suited to systems of low thermodynamic variance where the number of independent intensive variables is small.

The addition of mass balance equations to the Gibbs method permits the consideration of changes in extensive properties of the system such as moles of phases present. The mass balance constraints take the form

$$m_i = \sum_k M_k \sum_j v_{k,j,i} X_{k,j} \tag{4}$$

where m_i is the moles of the i^{th} system component, M_k is the moles of the k^{th} phase in the system, $v_{k,j,i}$ is the number of moles of the i^{th} system component in one mole of the j^{th} phase component in the k^{th} phase and $X_{k,j}$ is the mole fraction of the j^{th} phase component in the k^{th} phase. Because the Gibbs method employs the differential forms of the intensive thermodynamic variables, it is necessary to use the differential of the mass balance equations. The derivative of Eq. (4) is

$$dm_i = \sum_k dM_k \sum_j v_{k,j,i} X_{k,j} + \sum_k M_k \sum_j v_{k,j,i}\, dX_{k,j}. \tag{5}$$

Because only mole fractions of the independent phase components are variables in the Gibbs method, it is necessary to eliminate the derivative of the dependent mole fraction from Eq. (5), hence

$$dm_i = \sum_k dM_k \sum_j v_{k,j,i} X_{k,j} + \sum_k M_k \sum_j (v_{k,j,i} - v_{k,d,i})\, dX_{k,j} \tag{6A}$$

where $v_{k,d,i}$ is the number of moles of the i^{th} system component in the dependent phase component in the k^{th} phase. Equations (5) and (6A) are valid for either open or closed systems.

There is one equation of the form (6A) for each system component. In addition, Eqs. (6A) introduce as new variables the differentials of the moles of the phases in the assemblage (dM_k) and the differentials of the moles of system components (dm_i). The number of these new variables is equal to the number of phases plus the number of system components. Combining Eqs. (6A) with (1), (2) and (3), for a system containing NC system components, P phases and a total of NP phase components of which NX_j are independently variable, there are a total of $2+NP+NX_j+P+NC$ variables and $P+NP-NC+NX_j+NC=P+NP+NX_j$ equations. The difference between the number of variables and equations is $2+NC$.

Duhem's theorem states that for a closed system of known composition, only *two* variables are necessary to describe the equilibrium state of the system (Prigogine and Defay 1954). Incorporation of the notion embodied in Duhem's theorem into the Gibbs method requires that the bulk composition of the system be held constant. This requirement can be satisfied algebraically by setting $dm_i = 0$ in equations (6A), hence:

$$0 = \sum_k dM_k \sum_j v_{k,j,i} X_{k,j} + \sum_k M_k \sum_j (v_{k,j,i} - v_{k,d,i})\, dX_{k,j}. \tag{6B}$$

The variance of the system of equations resulting from the combination of (1), (2), (3) and (6B) is 2, which is consistent with Duhem's theorem. In general, the variance of the system of equations is equal to two plus the number of system components to which the system is open.

Equations (1), (2), (3) and (6A or 6B) may be solved in a variety of ways depending on the desired result. In general, solutions are obtained by making an arbitrary choice of independent variables and solving for changes in the remaining, dependent variables. Mathematically, this can be expressed as

$$\Theta_i = F(X_1, X_2, \ldots X_N) \tag{7}$$

where Θ_i is the dependent variable and X_1, $X_2 \ldots X_N$ are the independent variables. The total differential of (7) is

$$d\Theta_i = (\partial\Theta_i/\partial X_1)_{Xj\neq 1}\, dX_1 + (\partial\Theta_i/\partial X_2)_{Xj\neq 2}\, dX_2 + \ldots (\partial\Theta_i/\partial X_N)_{Xj\neq N}\, dX_N. \tag{8}$$

The change in dependent variable Θ may then be computed by solving for the derivatives $(\partial\Theta_i/\partial X_k)_{Xj\neq k}$ and multiplying by the change in the independent variable X_k.

For closed system behavior, the number of independent variables is 2, and results may be obtained by specifying changes in only 2, arbitrarily chosen variables. For example, if P and T are chosen as the independent variables, the changes in the compositions and modes of all phases can be computed for any change in P and T. Alternatively, the independent variables may be chosen to be compositional variables, such as $dX_{k,j}$, or modal variables such as dM_k. In this case, changes in mineral chemistry as deduced from chemical zoning profiles, mineral inclusion suites of fractionating phases, or changes in modal mineralogy as deduced from textural analysis, may be employed to monitor changes in P and T.

Systems undergoing fractional crystallization, such as crystals settling from a melt or metamorphic garnets undergoing growth zonation, can be modeled by setting the dm_i terms equal to the moles of component i lost to the fractionating phase. Alternatively, fractional crystallization can be modeled by noting that the mode of any phase undergoing fractional crystallization is always zero.

The methodology outlined above is fundamentally no different from other techniques to compute equilibrium phase assemblages, with one important distinction. Free energy minimization techniques, such as those presented by Brown and Skinner (1974), Ghiorso (1985), and Russell and Nicholls (1985) all require as input enthalpy, entropy, and volume data, activity models and the bulk composition of the system. Specification of the values of two independent variables is then sufficient to compute the values of all other variables. The primary difference between these approaches and the Gibbs method is that the latter utilizes the differential forms of the equilibrium thermodynamic and mass balance constraints, rather than the integrated forms of these equations. Consequently, enthalpy data are not required, which can be a major advantage because enthalpy data are often the most poorly constrained. Moreover, the equations of the Gibbs method are linear, so direct computation of changes in system variables can be made without iteration. Iteration is only required to ensure that the numerical integration of the system variables by Eqs. (8) from one set of values to another is numerically precise. The disadvantage of the Gibbs method is that there is no information

Table 1. System of linear differential equations for the assemblage quartz + pyroxene + olivine in the system $SiO_2-FeO-MgO$

$$\begin{bmatrix} S^{Qz} & -V^{Qz} & 1 & 0 & 0 & 0 & 0 & 0 & 0 & 0 & 0 & 0 \\ S^{Px} & -V^{Px} & 0 & X^{Px}_{En} & X^{Px}_{Fs} & 0 & 0 & 0 & 0 & 0 & 0 & 0 \\ S^{Ol} & -V^{Ol} & 0 & 0 & 0 & X^{Ol}_{Fo} & X^{Ol}_{Fa} & 0 & 0 & 0 & 0 & 0 \\ 0 & 0 & -1 & 4 & 0 & -3 & 0 & 0 & 0 & 0 & 0 & 0 \\ 0 & 0 & 0 & 2/3 & -2/3 & -1/2 & 1/2 & 0 & 0 & 0 & 0 & 0 \\ -(S^{Px}_{Fs}-S^{Px}_{En}) & (V^{Px}_{Fs}-V^{Px}_{En}) & 0 & 1 & -1 & 0 & 0 & G^{Px}_{22} & 0 & 0 & 0 & 0 \\ -(S^{Ol}_{Fa}-S^{Ol}_{Fo}) & (V^{Ol}_{Fa}-V^{Ol}_{Fo}) & 0 & 0 & 0 & 1 & -1 & 0 & G^{Ol}_{22} & 0 & 0 & 0 \\ 0 & 0 & 0 & 0 & 0 & 0 & 0 & 0 & 0 & 1 & 1/2 & 1/3 \\ 0 & 0 & 0 & 0 & 0 & 0 & 0 & -1/2\,M^{Px} & -2/3\,M^{Ol} & 0 & 1/2\,X^{Px}_{En} & 2/3\,X^{Ol}_{Fo} \\ 0 & 0 & 0 & 0 & 0 & 0 & 0 & 1/2\,M^{Px} & 2/3\,M^{Ol} & 0 & 1/2\,X_{Fs} & 2/3\,X^{Ol}_{Fa} \end{bmatrix} \begin{bmatrix} dT \\ dP \\ d\mu_{Qz} \\ d\mu^{Px}_{En} \\ d\mu^{Px}_{Fs} \\ d\mu^{Ol}_{Fo} \\ d\mu^{Ol}_{Fa} \\ dX^{Px}_{Fs} \\ dX^{Ol}_{Fa} \\ dM^{Qz} \\ dM^{Px} \\ dM^{Ol} \end{bmatrix} = \begin{bmatrix} 0 \\ 0 \\ 0 \\ 0 \\ 0 \\ 0 \\ 0 \\ 0 \\ 0 \\ 0 \\ 0 \\ 0 \end{bmatrix}$$

$G^{Px}_{22}=(\partial^2 G^{Px}/\partial(X^{Px}_{Fs})^2)_{P,T}$ $\quad G^{Ol}_{22}=(\partial^2 G^{Ol}/\partial(X^{Ol}_{Fa})^2)_{P,T}$

in the equations as to the relative stability of competing assembalges.

The philosophy inherent in applications of the Gibbs method is also somewhat different from that of techniques that incorporate the integrated forms of the thermodynamic equations. The Gibbs method is best suited to applications where the equilibrium state of the system is known or can be inferred from natural assemblages. In this case, nature provides the thermodynamic constant of integration (i.e. enthalpy) and an analysis of the phase relations can proceed from this reference point. Any changes in phase assemblage experienced by the rock must be inferred from the texture and chemistry of the phases (e.g. by an analysis of mineral zoning, inclusion suites of crystal fractionation sequences). The approach relies heavily on the petrographer's ability to decipher the paragenesis of a rock and less heavily on the quality of the thermodynamic data base.

Applications

The system $SiO_2-MgO-FeO$

Consider the assemblage quartz + orthopyroxene + olivine in the system $SiO_2-MgO-FeO$. The system of equations relating intensive variables in this assemblage were derived by Spear et al. (1982). The complete system of equations, incorporating the mass balance constraints, is shown here in Table 1. There are three phases, five phase components and two independent exchange potentials resulting in a total of twelve variables and ten equations. Note that conservative gram cation units have been used for the balanced stoichiometric relations and mass balance constraints. The input parameters necessary to solve these equations consist of the compositions ($X_{k,j}$), molar proportions of phases (M_k), molar entropies (S_k), molar volumes (V_k), exchange entropies and volumes (S_j-S_d; V_j-V_d) and the second derivative of the Gibbs free energy function at the pressure and temperature of interest.

In the examples discussed in this study, ideal solution models are assumed for all phases. With this assumption, the Gibbs function

$$G=\Sigma X_i \mu_i \tag{9}$$

may be readily differentiated to yield

$$(\partial^2 G/\partial X_i^2)_{P,T}=\alpha RT(1/X_i+1/X_d) \tag{10}$$

and

$$(\partial^2 G/\partial X_i\,\partial X_j)_{P,T}=\alpha RT/X_d \tag{11}$$

where X_d is the dependent mole fraction in the phase of interest and α is the crystallographic site multiplicity. The contribution to the curvature from nonideal mixing can also be readily incorporated if such terms are know. It should be noted that the equations presented in Tables 1 and 2 are completely general and make no assumptions as to thermodynamic data or solution models.

The equations in Table 1 may be solved in a variety of ways given the required input parameters. Bohlen and Boettcher (1981) report experimental data on this system, which indicate that at 900° C, 9.4 kb, the composition of orthopyroxene and olivine in equilibrium with quartz are $X_{Fs}=0.90$ and $X_{Fa}=0.951$, respectively. Using these values as a reference point and thermodynamic data of Helgeson et al. (1978) and Berman et al. (1986), the diagram in Fig. 1 was constructed. Isopleths of X_{Fs} in pyroxene have shallow positive slopes in agreement with the experimental results and extrapolation of Bohlen and Boettcher (1981). Isopleths of X_{Fa} in olivine are also shallow and slightly steeper than the X_{Fs} isopleths except in the limit where $X_{Fa}=X_{Fs}=1.0$.

Contours of the moles of olivine, pyroxene and quartz were computed from a system at 900° C, 9.4 kb, arbitrarily

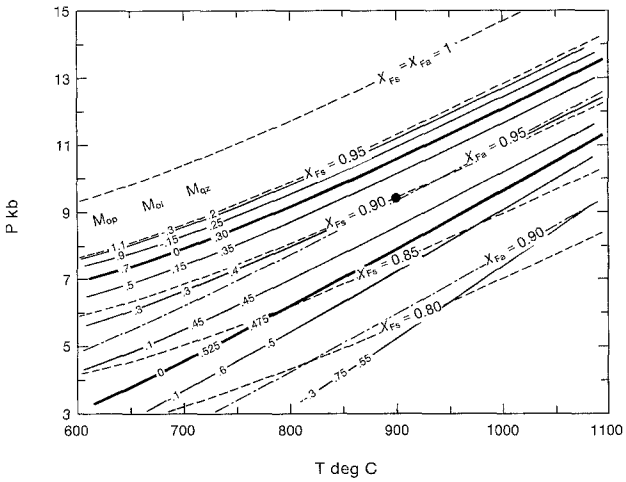

Fig. 1. $P-T$ diagram depicting contours of $X_{Fs,Px}$ (*dashed lines*) $X_{Fa,Ol}$ (*dot-dash lines*), M_{Qz}, M_{Ol} and M_{Px} (*solid lines*) for the assemblage orthopyroxene + olivine + quartz in the system $SiO_2-MgO-FeO$. Large dot depicts reference $P-T$ conditions ($T=900°$ C; $P=9.4$ kb, $X_{Fs,Px}=0.9$, $X_{Fa,Ol}=0.951$, $M_{Qz}=0.4$, $M_{Ol}=0.3$, and $M_{Px}=0.3$)

Table 2. System of linear differential equations for the assemblage olivine + melt in the system $SiO_2 - MgO - FeO$

$$\begin{bmatrix} S^{Ol} & -V^{Ol} & X^{Ol}_{Fs} & X^{Ol}_{Fa} & 0 & 0 & 0 & 0 & 0 & 0 & 0 & 0 \\ S^{M} & -V^{M} & 0 & 0 & X^{M}_{Mg} & X^{M}_{Fe} & X^{M}_{Si} & 0 & 0 & 0 & 0 & 0 \\ 0 & 0 & 1.5 & -1.5 & -1 & 1 & 0 & 0 & 0 & 0 & 0 & 0 \\ 0 & 0 & 3 & 0 & 2 & 0 & 1 & 0 & 0 & 0 & 0 & 0 \\ -(S^{Ol}_{Fa}-S^{Ol}_{Fo}) & (V^{Ol}_{Fa}-V^{Ol}_{Fo}) & 1 & -1 & 0 & 0 & 0 & G^{Ol}_{22} & 0 & 0 & 0 & 0 \\ -(S^{M}_{Fe}-S^{M}_{Mg}) & (V^{M}_{Fe}-V^{M}_{Mg}) & 0 & 0 & 1 & -1 & 0 & 0 & G^{M}_{22} & G^{M}_{23} & 0 & 0 \\ -(S^{M}_{Si}-S^{M}_{Mg}) & (V^{M}_{Si}-V^{M}_{Mg}) & 0 & 0 & 1 & 0 & -1 & 0 & G^{M}_{23} & G^{M}_{33} & 0 & 0 \\ 0 & 0 & 0 & 0 & 0 & 0 & 0 & 0M^{Ol} & 0M^{M} & M^{M} & 1/3 & X^{M}_{Si} \\ 0 & 0 & 0 & 0 & 0 & 0 & 0 & -2/3M^{Ol} & -M^{M} & -M^{M} & 2/3X^{Ol}_{Fo} & X^{M}_{Mg} \\ 0 & 0 & 0 & 0 & 0 & 0 & 0 & 2/3M^{Ol} & M^{M} & 0M^{M} & 2/3X^{Ol}_{Fa} & X^{M}_{Fe} \end{bmatrix} \begin{bmatrix} dT \\ dP \\ d\mu^{Ol}_{Fo} \\ d\mu^{Ol}_{Fa} \\ d\mu^{M}_{Mg} \\ d\mu^{M}_{Fe} \\ d\mu^{M}_{Si} \\ dX^{Ol}_{Fa} \\ dX^{M}_{Fe} \\ dX^{M}_{Si} \\ dM^{Ol} \\ dM^{M} \end{bmatrix} = \begin{bmatrix} 0 \\ 0 \\ 0 \\ 0 \\ 0 \\ 0 \\ 0 \\ 0 \\ 0 \\ 0 \\ 0 \\ 0 \end{bmatrix}$$

$G^{M}_{22} = (\partial^2 G^{M}/\partial(X^{M}_{Fe})^2)_{T,P}$ $\quad G^{M}_{23} = (\partial^2 G^{M}/\partial X^{M}_{Fe}\,\partial X^{M}_{Si})_{T,P}$
$G^{M}_{33} = (\partial^2 G^{M}/\partial(X^{M}_{Si})^2)_{T,P}$

consisting of 0.4 moles (48.7 volume %) quartz, 0.3 moles (24.8 volume %) olivine and 0.3 moles (26.5 volume %) of pyroxene. As can be seen, the mineral abundance isopleths have positive slopes that are very nearly parallel to the compositional isopleths for X_{Fs} and X_{Fa}. Isopleths for olivine, pyroxene and quartz are exactly parallel in this assemblage because only one net transfer reaction is possible. Mineral isopleths are not exactly parallel to composition isopleths because in addition to the net transfer reaction

Quartz + Fayalite = Ferosilite (12)

the exchange reaction

Fayalite − Forsterite = Ferosilite − Enstatite (13)

also occurs, which affects the slopes of composition isopleths but not mineral isopleths.

The assemblage quartz + pyroxene + olivine with initial molar ratios of 0.4, 0.3 and 0.3 respectively is not stable in all $P-T$ space. As reactions proceed, phases are consumed and the $P-T$ limit of the assemblage occurs where the amount of one or more phases equals 0. This, of course, depends on the initial bulk composition. The accessible limits of $P-T$ space for the initial conditions are shown by heavy lines in Fig. 1. Thompson et al. (1982) and Thompson (1982) have described the area (or volume) accessible to an assemblage as the reaction polygon.

The slopes and spacing of mineral abundance isopleths are also a function of the initial bulk composition of the rock. For the phase proportions at 900° C, 9.4 kb considered above, computed slopes are $(dP/dT)_{MPx} = 15.2$ bars/deg and $(dP/dM_{Px})_T = 3750$ bars/mole fraction. For an assemblage consisting of 0.8 moles of quartz, 0.2 moles of olivine and 0.0 moles of pyroxene at 900° C, 9.4 kb, these slopes are 16.6 bars/deg and 13660 bars/mole fraction, respectively.

Olivine-melt equilibria. The equilibrium between olivine and melt in the system $SiO_2 - MgO - FeO$ is an example of a system with a higher thermodynamic variance. The system of equations for this assemblage is shown in Table 2. Note that because the melt is a ternary solution, both curvatures and cross curvatures of the Gibbs function are required to define the exchange potentials (Eqs. 3).

Isopleths of melt and olivine composition and moles of melt and olivine are depicted in Fig. 2, using the input parameters specified in the figure caption. As can be seen, isopleths of mineral and melt composition are steep and nearly parallel owing to the relatively large entropy of the melt compared to olivine, and the relatively small ΔS of exchange. With decreasing T at constant P, both $X(SiO_2)$ in the melt and X_{Fa} in olivine increase monotonically. X_{FeO} in the melt, however, first increases to a maximum at approximately 0.243 and then decreases with decreasing T, although Fe/Mg increases monotonically.

In Fig. 3 are plotted two computed isobaric liquid lines of descent along with the composition of coexisting olivine. The first (Fig. 3A) shows the liquid line of descent under conditions of continual olivine-liquid equilibrium. As expected, the tie lines between olivine and melt pivot on the bulk composition. The maximum in X_{FeO} in the melt is also readily apparent in this plot. In Fig. 3B, the liquid line of descent under conditions of fractional crystallization of olivine is plotted. Again, as expected, the trends of both the melt and the olivine are towards considerably more Fe-rich compositions than in the equilibrium crystallization model, although the melt is not as silicic for a given change in T. Also, the maximum in $X_{FeO,Melt}$ is shifted to slightly higher values (0.265) and lower temperatures.

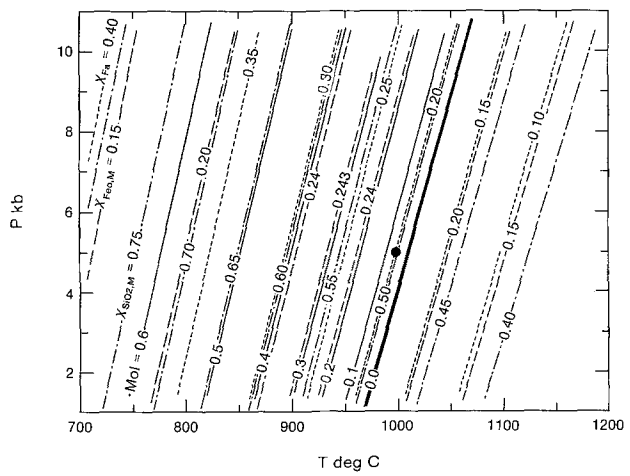

Fig. 2. $P-T$ diagrams depicting contours of $X_{Fa,Ol}$ (*dotted lines*), $X_{FeO,Melt}$ (*dashed lines*), $X_{SiO_2,Melt}$ (*dot-dash lines*) and M_{Ol} (*solid lines*) for the assemblage olivine + melt in the system $SiO_2 - MgO - FeO$. Reference conditions (*large dot*) are $P = 5$ kb, $T = 1000°$ C, $X_{Fa,Ol} = 0.2$, $X_{FeO,Melt} = 0.227$, $X_{SiO_2,Melt} = 0.5$, $M_{Ol} = 0.05$, $M_{Melt} = 0.95$

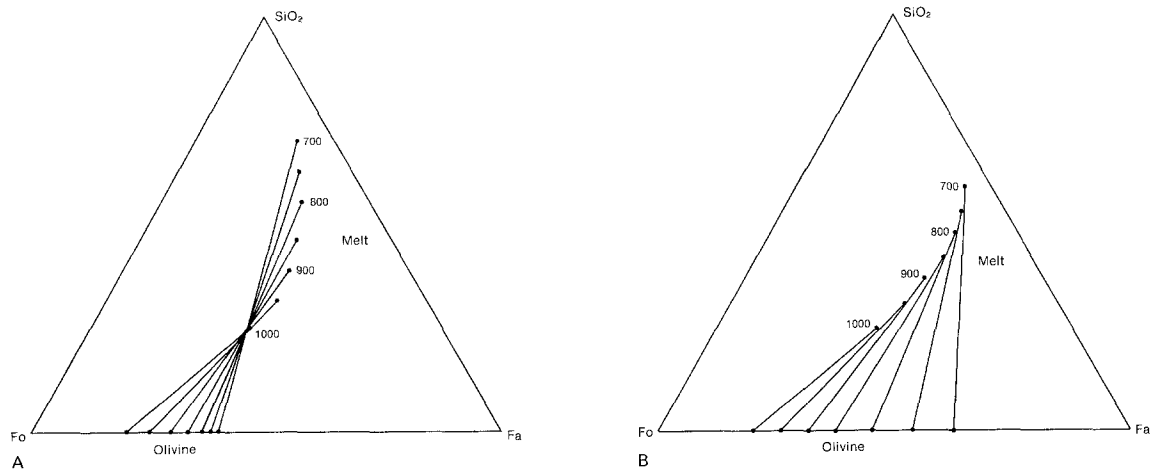

Fig. 3A, B. Ternary $Fe_2SiO_4-Mg_2SiO_4-SiO_2$ diagrams depicting the evolution of melt and olivine composition with isobaric cooling from the initial conditions specified in *Fig. 2. Tie lines* connect coexisting olivine and melt at different temperatures. **A** Equilibrium crystallization; **B** Fractional crystallization of olivine

Pelitic Schists

Consider the assemblage garnet + biotite + staurolite + quartz + muscovite + fluid (H_2O) in the system $SiO_2-Al_2O_3-FeO-MgO-K_2O-H_2O$ (KFMASH). Garnet, biotite and staurolite ($Fe_2Al_9Si_{3.75}O_{22}(OH)_2$) are assumed to be binary Fe–Mg solutions and quartz, muscovite and fluid are assumed to be pure. With these assumptions, there are two independent exchange reactions

$$FeMg_{-1}(\text{garnet}) = FeMg_{-1}(\text{biotite}) \quad (14)$$

$$FeMg_{-1}(\text{garnet}) = FeMg_{-1}(\text{staurolite}) \quad (15)$$

and one net transfer reaction (balanced for gram-cation units)

$$0.913\ \text{staurolite} + 1\ \text{biotite} + 0.232\ \text{quartz} = 0.579\ \text{garnet} + 0.889\ \text{muscovite} + 0.058\ H_2O. \quad (16)$$

The results of calculations for this assemblage are presented in Fig. 4 as isopleths of X_{Fe} in garnet, biotite and staurolite and of moles of garnet. According to the petrogenetic grid of Spear and Cheney (1986), the limiting reactions for the assemblage garnet + biotite + staurolite are the two KFMASH reactions chloritoid + muscovite + quartz = garnet + biotite + staurolite + H_2O and staurolite + muscovite + quartz = garnet + biotite + Al_2SiO_5 + H_2O and the KFASH reaction Fe-staurolite + annite + quartz = almandine + muscovite + H_2O. Isopleths of X_{Fe} in garnet, biotite and staurolite must necessarily start at the limiting KFASH reaction with values of 1.0 and decrease with increasing temperature and/or pressure. The isopleths are not exactly parallel for the three minerals owing to the interactions of the two exchange reactions and the net transfer reaction on the mineral compositions. Garnet has the steepest isopleth, then staurolite with biotite showing the shallowest.

Isopleths of garnet abundance were computed by assuming initial molar ratios for each phase as indicated in the figure caption at a pressure and temperature of 7 kb and 620° C and mineral compositions consistent with these conditions (the large dot in Fig. 4). The contour for $M_{Gar}=0$ therefore passes through this $P-T$ point. Contours for $+M_{Gar}$ signify garnet growth whereas contours for $-M_{Gar}$ signify garnet consumption. The amounts of all other phases also change across the mineral isopleths by an amount exactly specified by the stoichiometric ratios in the net transfer reaction (Eq. 16).

The contours for M_{Gar} may be interpreted as the $P-T$ trace of the net transfer reaction (Eq. 16). In the limit as X_{Fe} approaches 1.0 in each of the phases, these contours must become parallel to the KFASH limiting reaction. The mineral isopleths are not necessarily parallel to any of the composition isopleths because composition isopleths are governed by the exchange equilibria in addition to the net transfer reaction.

As an example of a natural pelite, consider again the assemblage garnet + biotite + staurolite + quartz + mus-

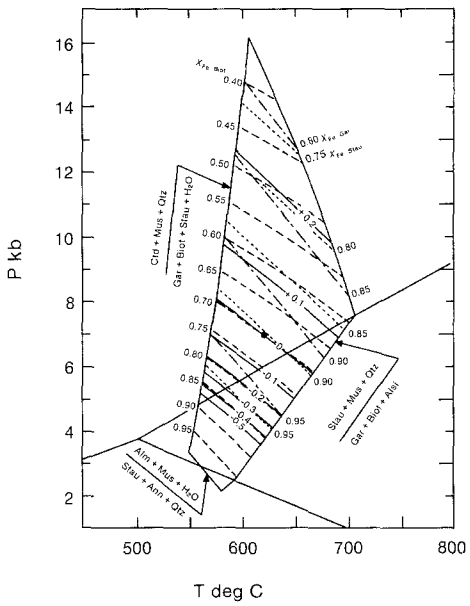

Fig. 4. $P-T$ diagram depicting contours of $X_{Fe,Gar}$ (*dot-dashed lines*), $X_{Fe,Biot}$ (*dashed lines*), $X_{Fe,Stau}$ (*dotted lines*) and M_{Gar} (*solid lines*). The reference point for constructing composition isopleths is $X_{Fe,Gar}=X_{Fe,Biot}=X_{Fe,Stau}=1.0$ along the KFASH limiting reaction Stau + Ann + Qtz = Alm + Mus + H_2O. The reference point for mineral abundance isopleths (*large dot*) is $P=7$ kb, $T=620°$ C, $X_{Fe,Gar}=0.927$, $X_{Fe,Biot}=0.702$, $X_{Fe,Stau}=0.904$, $M_{Qz}=0.25$, $M_{H_2O}=0.0$, $M_{Mus}=0.25$, $M_{Gar}=0.0$, $M_{Biot}=0.25$, $M_{Stau}=0.25$

Table 3. Initial conditions at $T=520°$ C, $P=3.5$ kb for calculations involving the assemblage garnet + biotite + staurolite + muscovite + quartz + plagioclase + fluid (H_2O) in the system MnNCKFMASH

Phase	Moles	X_{Fe}	X_{Mn}	X_{Ca}
Quartz	0.20	–	–	–
H_2O	0.0	–	–	–
Muscovite	0.25	–	–	–
Plagioclase	0.10	–	–	0.243[a]
Garnet	0.15	0.682	0.161	0.038
Biotite	0.20	0.463	0.003	–
Staurolite	0.10	0.793	0.028	–

[a] $X_{anorthite}$

covite + fluid (H_2O) with plagioclase in the system $SiO_2-Al_2O_3-MgO-FeO-MnO-CaO-Na_2O-K_2O-H_2O$ (MnNCKFMASH). In addition to reactions 14, 15, and 16, two additional exchange reactions

$$FeMn_{-1}(\text{garnet}) = FeMn_{-1}(\text{biotite}) \quad (17)$$

$$FeMn_{-1}(\text{garnet}) = FeMn_{-1}(\text{staurolite}) \quad (18)$$

and the net transfer reaction (balanced for gram-cation units)

$$1.667 \text{ anorthite} + 1.0 \text{ annite} = 0.889 \text{ grossular} + 0.889 \text{ almandine} + 0.889 \text{ muscovite} \quad (19)$$

may also be written.

The thermodynamic variance of this assemblage is 4; however, employing mass balance constraints and the assumption of closed system behavior, isopleths may be computed for any phase as shown in Figs. 5 and 6. Initial conditions for these calculations are from a natural schist from Mt Moosilauke, New Hampshire (Hodges and Spear, 1982) and are given in Table 3. Isopleths of X_{Alm} in garnet (Fig. 5A) have generally negative slopes, similar to the results obtained for KFMASH system, but there X_{Alm} displays a maximum. Contours of X_{Spes} (Fig. 5D) have similar slopes and decrease monotonically. The maximum in almandine composition occurs because the temperature of the dominant net transfer reaction (Eq. 16) in the KFASH system is intermediate between that of the KMnASH and KMASH systems, which are lower and higher, respectively. Almandine content therefore increases largely by virtue of Fe–Mn equilibria and then decreases by Fe–Mg equilibria. In fact, the maximum in X_{Alm} is very near the $P-T$ conditions of the KFASH reaction.

Isopleths for X_{Anor} (Fig. 5B) are relatively flat with X_{Anor} decreasing with increasing P. Contours of X_{Gros} (Fig. 5B) have positive slopes at low pressures, but become nearly

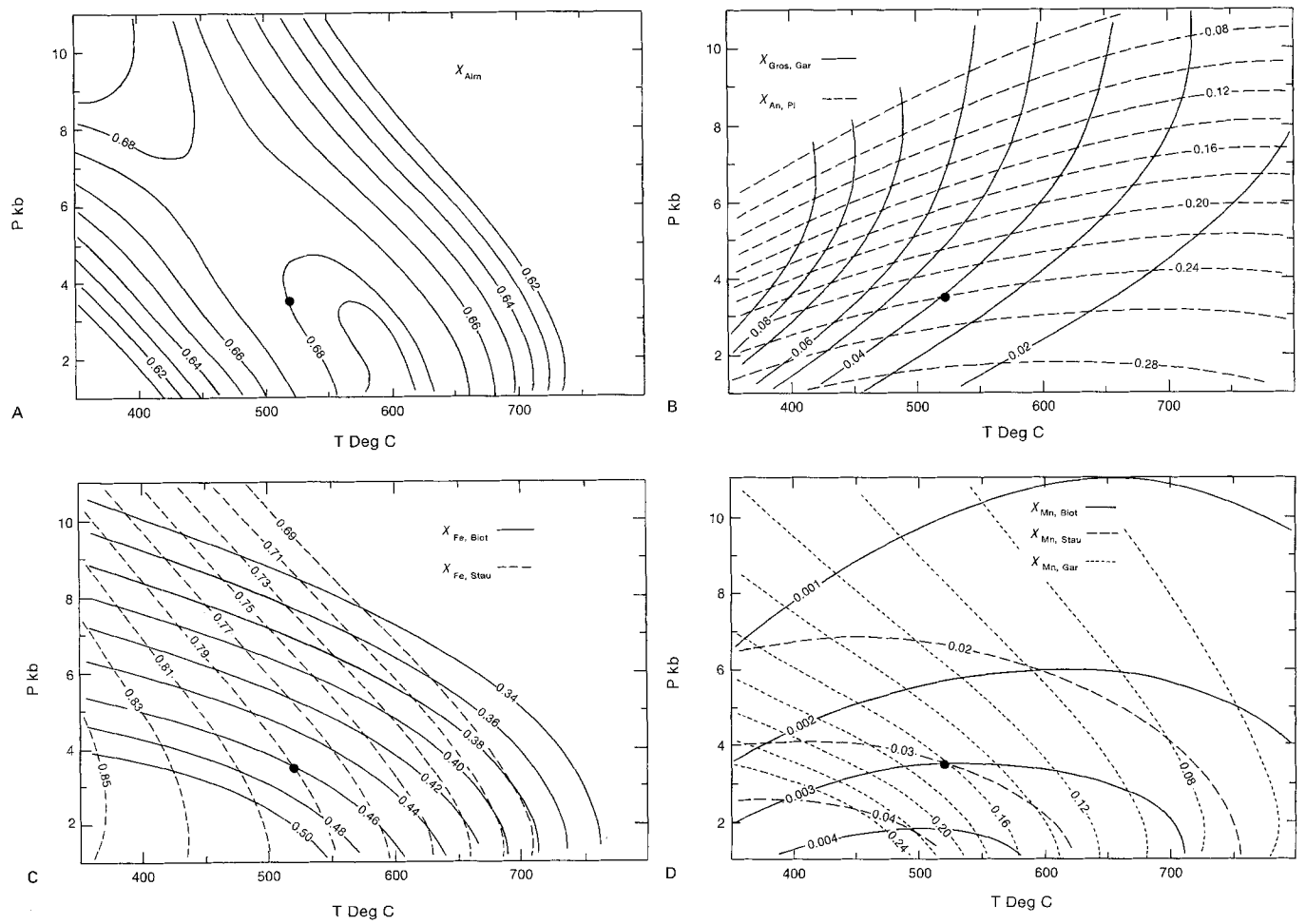

Fig. 5A–D. $P-T$ diagrams depicting isopleths of garnet, biotite, staurolite and plagioclase composition for the assemblage garnet + biotite + staurolite + muscovite + quartz + plagioclase + fluid (H_2O) in the system MnNCKFMASH. Reference conditions (*large dot*) are given in *Table 3*. **A** Isopleths of $X_{Fe,Gar}$; **B** Isopleths of $X_{Ca,Gar}$ and $X_{Anor,Plag}$; **C** Isopleths of X_{Fe} in biotite and staurolite; **D** Isopleths of X_{Mn} in garnet, staurolite and biotite

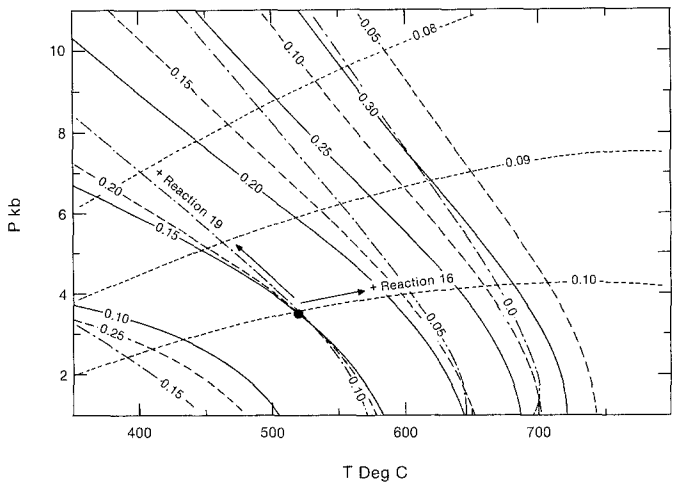

Fig. 6. Mineral abundance isopleths of garnet (*solid lines*), biotite (*dashed lines*), staurolite (*dot-dashed lines*) and plagioclase (*dotted lines*) for the system depicted in *Fig. 5* and *Table 3*. Large dot shows references $P-T$ conditions

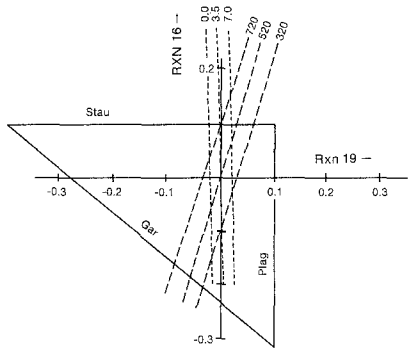

Fig. 7. Reaction space contoured for P (*dotted lines*) and T (*dashed lines*) for the system depicted in *Fig. 5* and *6* and *Table 3*. *Solid line* delimits the "reaction polygon", which limits the accessible portion of reaction space for this assemblage

vertical at high pressures and low temperatures. Both X_{Gros} and X_{Anor} are controlled only by reaction 13. However, also involved in this reaction are the activities of annite and almandine, which also vary with P and T. Isopleths of X_{Fe} and X_{Mn} in biotite and staurolite (Figs. 5C and D) have negative slopes and vary monotonically, although the slopes are quite different in each phase.

Four sets of mineral abundance isopleths are shown in Fig. 6. Plagioclase contours are relatively flat with M_{Plag} decreasing with increasing pressure. Inasmuch as net transfer reaction 19 is the only reaction governing both plagioclase composition and modes, the contours for X_{Anor} and M_{Plag} must necessarily be parallel. Contours for moles of biotite and moles of muscovite must also be parallel, as must contours for moles of staurolite, quartz and H_2O, because the production and consumption of these phases are governed by the stoichiometries of the two net transfer reactions. Mineral abundance contours for garnet, biotite-muscovite and staurolite-quartz-H_2O have relatively steep negative slopes that reflect the negative slope of the net transfer reaction, equation 16. They are not parallel to any composition isopleths because the latter are also governed by the exchange equilibria.

Applications of the reaction progress variable to metamorphic petrology have been discussed by Ferry (1983), Thompson et al. (1982), Rice and Ferry (1982), Thompson (1982), Kimball et al. (1985) and others. In the above example, reaction progress of the two net transfer reactions may be monitored by the changes in the moles of one or more phases. Reaction 16 does not involve the production or consumption of plagioclase, therefore progress along this reaction must be parallel to isopleths of plagioclase abundance (dashed lines in Fig. 6). Similarly, reaction 19 does not involve the production or consumption of staurolite, quartz and H_2O so progress along this reaction must be parallel to isopleths of staurolite-quartz-H_2O abundance (dot-dashed lines in Fig. 6). With these considerations, the direction of reaction progress may be specified as labeled in Fig. 6.

An alternative way of viewing reaction progress is by plotting a reaction space, where the reaction coordinates have been rendered orthogonal, as shown in Fig. 7 (cf. Thompson, 1982; Rice and Ferry, 1982). $P-T$ contours have been drawn on this diagram by solving the system of equations for $(dM_{Stau}/dM_{Plag})_T$ and $(dT/dM_{Stau})_{MPlag}$ etc. It should be noted that isopleths of mineral composition may also be contoured on this diagram by derivation of quantities such as $(dM_{Stau}/dM_{Plag})_{X(Fe,Gar)}$, etc.

The reaction polygon, as defined by Thompson et al. (1982), defines the limit of accessible $P-T$ space for an assemblage. Along each face of the reaction polygon the moles of a phase in the assemblage equals 0. In Fig. 7 the reaction polygon is shown as solid lines labeled with the phase that is of zero quantity along the respective face. In Fig. 6, the reaction polygon may be deduced by identification of mineral abundance isopleths where the moles of the phase equals 0. It is interesting to note that for the assemblage garnet + biotite + staurolite + quartz + muscovite + plagioclase + H_2O, only the staurolite-out face of the reaction polygon plots on the $P-T$ diagram of Fig. 6 (compare P and T contours on Fig. 7 with Fig. 6); other faces of the reaction polygon plot at either very high pressure or low temperature.

Discussion

Systems of equations that describe the exact thermodynamic constraints among the differentials of intensive and extensive variables of a system can be a tremendous aid in helping to decipher petrogenetic processes. Because the equations involve the differentials of the thermodynamic variables, the methodology is only suited to the calculations of *changes* in these variables from a reference state to another set of conditions. Moreover, because the equations are linear, solution to the equations can be computed directly by Gaussian elimination.

As the preceding examples indicate, the methodology may be applied to the contouring of any thermodynamic variable against any others. In addition, it is also possible to track the composition and modes of phases along a prescribed pressure-temperature path, or alternatively to use changes in phase compositions or modes to infer changes in pressure and temperature. Spear and Selverstone (1983) have described such an application where the compositional growth zoning preserved in garnet is used to infer pressure-temperature paths of crystallization. In that method, only the intensive variables of the system (i.e. no mass balance constraints) are considered and application of the technique

is limited to assemblages of relatively low thermodynamic variance (in practice, quadravariant or lower). However, by assuming closed system behavior, or open system behavior where mass transfer is characterized quantitatively (e.g. a fractional crystallization model), then the number of degrees of freedom of any system is two. This approach might have considerable application in igneous petrology where compositional trends of melts may be inferred by analysis of a suite of igneous rocks and it is desired to know the $P-T$ evolution responsible for these trends. Other applications include the calculation of the liquid line of descent or compositional evolution of a zoned garnet along a prescribed $P-T$ trajectory.

Applications involving reaction progress form an important link between petrographic observations of modal changes and chemical changes that occur in phases. Diagrams such as Fig. 6 may, therefore, be a useful aid for deciphering the $P-T$ evolution of a rock. For example, if accurate modal changes can be measured then a unique $P-T$ path can be inferred. In practice, some phases will be better monitors than others; in the example in Fig. 6, plagioclase modes in addition to any other phase would provide the best resolution of both pressure and temperature, but any other pair (exclusive of plagioclase) would not because of the low angle of intersection of mineral abundance isopleths. Combinations of modal and chemical changes would permit evaluation of the degree to which a system is open to various chemical species.

Acknowledgments. This work was supported by National Science Foundation grants EAR-8514659 and EAR-8708609. A constructive review by J.M. Ferry is gratefully acknowledged.

References

Berman RG, Engi M, Greenwood HJ, Brown TH (1986) Derivation of internally-consistent thermodynamic data by the technique of mathematical programming: a review with application to the system $MgO-SiO_2-H_2O$. J Petrol 27:1143–1364

Bohlen SR, Boettcher AL (1981) Experimental investigations and geological applications of orthopyroxene geobarometry. Am Mineral 66:951–964

Brown TH, Skinner BJ (1974) Theoretical prediction of equilibrium phase assemblages in multicomponent systems. Am J Sci 274:961–986

Ferry JM (1983) On the control of temperature, fluid composition, and reaction progress during metamorphism. Am J Sci 283-A:201–232

Ghiorso MS (1985) Chemical mass transfer in magmatic processes. I. Thermodynamic relations and numerical algorithms. Contrib Mineral Petrol 90:107–120

Helgeson HC, Delany JM, Nesbitt HW, Bird DK (1978) Summary and critique of the thermodynamic properties of rock-forming minerals. Am J Sci 278A:1–299

Hodges KV, Spear FS (1982) Geothermometry, geobarometry and the Al_2SiO_2 triple point at Mt. Moosilauke, New Hampshire. Am Mineral 67:1118–1134

Kimball KL, Spear FS, Dick HJB (1983) High temperature alteration of abyssal ultramafics from the Islas Orcadas Fracture Zone, South Atlantic. Contrib Mineral Petrol 91:307–320

Prigogine I, Defay R (1954) Chemical Thermodynamics. Longmans, Green and Co., London

Rice JM, Ferry JM (1982) Buffering, infiltration and the control of intensive variables during metamorphism. In: Ferry JM (ed) Characterization of Metamorphism through Mineral Equilibria. Mineral Soc Am [Reviews in Mineral] 10:263–326

Russell JK, Nicholls J (1985) Application of Duhem's theorem to the estimation of extensive and intensive properties of basaltic magmas. Can Mineral 23:479–488

Spear FS, Cheney JT (1986) Yet another petrogenetic grid for pelitic schists. Geol Soc Am Abstracts with Programs 18:758

Spear FS, Ferry JM, Rumble D (1982) Analytical formulation of phase equilibria: The Gibbs method. In: Ferry JM (ed) Characterization of Metamorphism through Mineral Equilibria. Mineral Soc Am [Reviews in Mineral] 10:105–152

Spear FS, Selverstone J (1983) Quantitative $P-T$ paths from zoned minerals: Theory and tectonic applications. Contrib Mineral Petrol 83:348–357

Thompson JB (1982) Reaction space: an algebraic and geometric approach. In: Ferry JM (ed) Characterization of Metamorphism through Mineral Equilibria. Mineral Soc Am [Reviews in Mineral] 10:33–51

Thompson JB, Laird J, Thompson AB (1982) Reactions in amphibolite, greenschist and blueschist. J Petrol 23:1–17

Received July 6, 1987 / Accepted March 14, 1988
Editorial responsibility: I.S.E. Carmichael